Regulation of mitochondrial morphology by APC/C^Cdh1-mediated control of Drp1 stability

Sarah R. Horn[a], Michael J. Thomenius[a], Erika Segear Johnson[a], Christopher D. Freel[a], Judy Q. Wu[a,b], Jonathan L. Coloff[a,c,d,e], Chih-Sheng Yang[a], Wanli Tang[a], Jie An[a,d], Olga R. Ilkayeva[a,d], Jeffrey C. Rathmell[a,c,d], Christopher B. Newgard[a,d], and Sally Kornbluth[a]

[a]Department of Pharmacology and Cancer Biology, Duke University Medical Center, Durham, NC 27710; [b]Carolina Cardiovascular Biology Center, University of North Carolina, Chapel Hill, NC 27599; [c]Department of Immunology and [d]Sarah W. Stedman Nutrition and Metabolism Center, Duke University Medical Center, Durham, NC 27710; [e]Department of Cell Biology, Harvard Medical School, Boston, MA 02115

ABSTRACT Homeostatic maintenance of cellular mitochondria requires a dynamic balance between fission and fusion, and controlled changes in morphology are important for processes such as apoptosis and cellular division. Interphase mitochondria have been described as an interconnected network that fragments as cells enter mitosis, and this mitotic mitochondrial fragmentation is known to be regulated by the dynamin-related GTPase Drp1 (dynamin-related protein 1), a key component of the mitochondrial division machinery. Loss of Drp1 function and the subsequent failure of mitochondrial division during mitosis lead to incomplete cytokinesis and the unequal distribution of mitochondria into daughter cells. During mitotic exit and interphase, the mitochondrial network reforms. Here we demonstrate that changes in mitochondrial dynamics as cells exit mitosis are driven in part through ubiquitylation of Drp1, catalyzed by the APC/C^Cdh1 (anaphase-promoting complex/cyclosome and its coactivator Cdh1) E3 ubiquitin ligase complex. Importantly, inhibition of Cdh1-mediated Drp1 ubiquitylation and proteasomal degradation during interphase prevents the normal G1 phase regrowth of mitochondrial networks following cell division.

INTRODUCTION

Through posttranslational modifications of mitochondrial morphology–controlling proteins like (dynamin-related protein 1) Drp1, mitochondrial fission and fusion are coordinated with key cellular events (reviewed in Benard and Karbowski, 2009). Phosphorylation, sumoylation, nitrosylation, and ubiquitylation have been reported to affect various aspects of Drp1 function, including its localization, stability, and GTPase activity (Harder *et al.*, 2004; Chang and Blackstone, 2007; Cribbs and Strack, 2007; Karbowski

et al., 2007; Taguchi *et al.*, 2007; Wasiak *et al.*, 2007; Han *et al.*, 2008; Cho *et al.*, 2009; Zunino *et al.*, 2009). The yeast mitofusin homologue Fzo1p undergoes proteasomal degradation, and increasing evidence supports a role for mammalian E3 ubiquitin ligases in the regulation of mitochondrial fission and fusion as well (Fritz *et al.*, 2003; Escobar-Henriques *et al.*, 2006; Nakamura *et al.*, 2006; Yonashiro *et al.*, 2006; Neutzner *et al.*, 2008; Amiott *et al.*, 2009; Park *et al.*, 2010).

During the cell cycle, Drp1-mediated mitochondrial fission is essential for the completion of cytokinesis and for the proper distribution of mitochondria into the daughter cells (Labrousse *et al.*, 1999; Okamoto and Shaw, 2005; Taguchi *et al.*, 2007; Ishihara *et al.*, 2009). In interphase cells, mitochondria have been described as an interconnected network that begins to fragment as the cells enter mitosis (Barni *et al.*, 1996; Margineantu *et al.*, 2002; Taguchi *et al.*, 2007). Mitochondrial fragmentation at the time of mitotic entry is known to be regulated by Cdk1/cyclin B–mediated phosphorylation and SenP5-mediated deSUMOylation of Drp1 (Taguchi *et al.*, 2007; Zunino *et al.*, 2009). During telophase and cytokinesis of mitotic exit, reestablishment of the fused mitochondrial network (and mitochondrial elongation)

FIGURE 1: Stability of Drp1 changes during the cell cycle. (A) Prometaphase-arrested HeLa cells were collected at the indicated times after nocodazole release. Actin is shown as a loading control, and phospho-Histone H3 is a mitotic marker. (B) Quantification of data shown in (A), n = 3. Drp1 protein levels were quantified and normalized to actin levels in three independent experiments. The results are plotted as a percentage of Drp1 remaining at 3, 5, and 7 h following release from nocodazole arrest, with 100% representing the Drp1 level at time 0. The error bars reflect the SE of the mean. (C) HeLa S3 cells were released from thymidine-induced G1/S arrest into medium containing nocodazole and were collected at the indicated times. (D) HeLa cells were released from thymidine-induced G1/S arrest as in (C), and lysates were probed for the indicated mitochondrial morphology proteins. (E) Autoradiograms of ^{35}S-labeled Drp1 after incubation with HeLa cell extracts prepared 2 h after release from nocodazole arrest, or from HeLa cells arrested in prometaphase with nocodazole. (F) Quantification of data shown in (E), n = 5. Differences in the percentage of ^{35}S-Drp1 remaining in G1 lysates vs. the mitotic lysates at time points 60 and 120 min are statistically significant by Student's *t* test (*p = 0.013079; **p = 0.013553).

occurs, and interphase mitochondria once again form an extensive network (Taguchi *et al.*, 2007; Mitra *et al.*, 2009). Significant increases in mitochondrial membrane potential and respiration occur during progression through G1, and the presence of a hyperfused mitochondrial network is necessary for cyclin E accumulation and cell-cycle progression (Taguchi *et al.*, 2007; Schieke *et al.*, 2008; Mitra *et al.*, 2009).

Given the dramatic shift in morphology from fragmented mitochondria in mitosis to a predominantly elongated mitochondrial network during interphase, we wanted to determine whether alterations in Drp1 also contributed to changes in mitochondrial morphology as cells exited mitosis and entered G1. On the basis of the importance of ubiquitin-dependent degradation in coordinating key cell-cycle transitions, we questioned whether the dramatic changes in mitochondrial morphology that occur as cells undergo division are regulated by proteolytic degradation of Drp1. We show here that this is, indeed, the case and that cell-cycle–dependent degradation depends on the anaphase-promoting complex/cyclosome (APC/C), a central coordinator of events at the M/G1 transition.

RESULTS

Drp1 levels decrease upon release from mitotic arrest

We examined the stability of Drp1 during cell-cycle progression and found that Drp1 levels dropped when cells were released from a nocodazole-induced prometaphase arrest, as the cells exited mitosis and entered G1 (Figure 1, A and B). Additionally, levels of Drp1 gradually increased as HeLa cells entered mitosis following release from a double thymidine block (G1/S arrest), whereas levels of several other proteins involved in the regulation of mitochondrial morphology did not change (Figure 1, C and D). We noted that this down-regulation of Drp1 temporally coincides with the return of mitochondria to a reticular network from their predominantly fragmented mitotic morphology (Supplemental Movie S1). Additionally, we found that in vitro–translated ^{35}S-Drp1 was degraded in cell extracts prepared from synchronized G1 cells, whereas Drp1 was stable in lysates prepared from prometaphase-arrested cells (Figure 1, E and F).

In an in vitro mitotic exit assay, Drp1 protein levels decreased, whereas blocking mitotic exit with addition of the APC/C inhibitory protein Emi2 attenuated Drp1 degradation (Figure 2A).
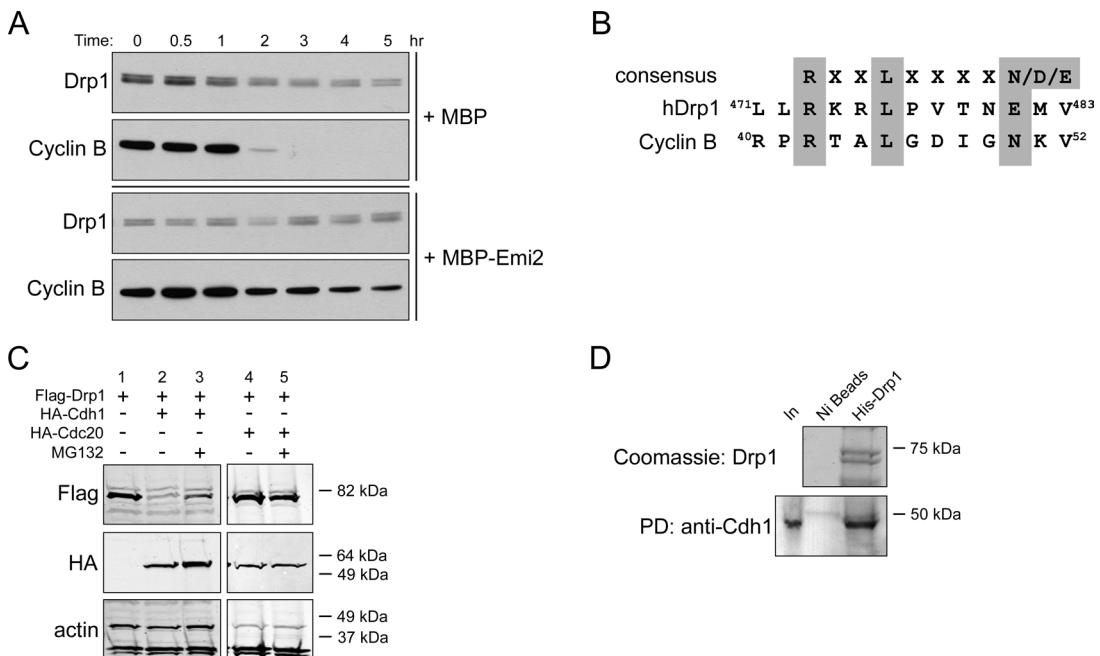
FIGURE 2: Drp1 degradation is stimulated by Cdh1. (A) HeLa cells were arrested with nocodazole and then cultured in fresh medium for 1 h. Hypotonic cell lysates were incubated at room temperature, and aliquots were taken at the indicated times for immunoblotting. In the bottom panel, MBP-Emi2 was added to cell lysates before incubation at room temperature. (B) Alignment of D-Boxes in Drp1 and cyclin B1. (C) Expression of FLAG-tagged Drp1 with or without HA-Cdh1 or HA-Cdc20 in HEK 293T cells, in the absence or presence of the proteasome inhibitor MG132. (D) Ni-beads or Ni-beads conjugated to His-tagged Drp1 were incubated with HEK 293T cell lysates, and the beads were immunoblotted for Cdh1. The input lane represents 10% of the lysate used in the pull down.

On the basis of the timing of Drp1 degradation and the ability of Emi2 to interfere with this degradation, we examined the possibility that Drp1 might be ubiquitylated by the APC/C ubiquitin ligase, an E3 complex active during mitotic exit and the G1 phase of the cell cycle. In this regard, we were interested to find that Drp1 contains multiple APC/C degradation motifs, including a canonical degradation box (D-Box) motif (R-X-X-L-X-X-X-X-N/D/E), suggesting that it might be a substrate of the APC/C (Figure 2B).

Drp1 is a novel substrate of APC/C

Drp1 levels are lowest during the G1 phase of the cell cycle, when the APC/C is active through its association with Cdh1. We examined the effect of overexpression of the APC/C coactivator proteins Cdc20 and Cdh1 on Drp1 levels and found that Cdh1 expression resulted in a significant decrease in steady-state levels of Drp1 (Figure 2C). Importantly, this decrease in Drp1 was attenuated by treatment with the proteasome inhibitor MG132, and we detected binding between Drp1 and Cdh1 in cell lysates (Figure 2D).

On the basis of the role of Drp1 in mediating fission of mitochondria, we examined mitochondrial morphology in cells overexpressing Cdh1 and found that overexpression of Cdh1 results in a range of alterations in mitochondrial morphology that are consistent with increased mitochondrial connectivity, stemming from either decreased mitochondrial fission or increased mitochondrial fusion (Figures 3A and Supplemental Figure 1). Indeed, when we measured the rate of mitochondrial fusion using diffusion of photoactivatable mito-green fluorescent protein (mito-GFP), we observed a more rapid diffusion of GFP in cells expressing Cdh1 compared with vector control, consistent with decreased mitochondrial fission and increased mitochondrial fusion (Figure 3B).

Drp1 D-Box contributes to APC/C^Cdh1-mediated ubiquitylation and degradation

To examine the contribution of the putative Drp1 D-Box to Drp1 degradation by APC/C^{Cdh1}, we performed in vitro ubiquitylation assays using wild-type (WT) Drp1 or a Drp1 in which two key D-box residues had been mutated to alanines (RxxL to AxxA). When supplemented with recombinant Cdh1 (but not Cdc20), APC complexes immunoprecipitated from interphase extracts prepared from *Xenopus* eggs (a rich source of APC components) promoted polyubiquitylation of WT Drp1, whereas ubiquitylation of Drp1 containing a mutant D-Box motif was attenuated, but not completely abolished (Figure 4, A and B; see more in HeLa cells). We next compared the expression of Drp1 WT to the Drp1 D-Box mutant during G1 phase and found that the amount of D-Box mutant protein remaining after release from nocodazole arrest was increased relative to the WT protein (Figure 4C). Although levels of the D-Box mutant were stabilized during G1 relative to the WT protein, partial degradation of the D-Box mutant still occurred, suggesting that additional APC targeting motifs may be required for full degradation, as is the case for other for APC/C^{Cdh1} substrates, such as Claspin and Aurora A (Crane *et al.*, 2004; Bassermann *et al.*, 2008).

Although the D-Box that we initially identified most closely aligns with the canonical motif (R-X-X-L-X-X-X-X-N/D/E), upon close examination of the Drp1 protein sequence, we noted that it contains several previously described degrons for APC/C substrates, including nine canonical RxxL motifs as well as noncanonical, motifs such as a GxEN box and an O-Box (Castro *et al.*, 2003; Araki *et al.*, 2005), and it is likely that multiple degrons are necessary for full Drp1 degradation by APC/C^{Cdh1}.

Because even moderate overexpression of WT Drp1 alone is sufficient to induce mitochondrial fragmentation, we anticipated that it
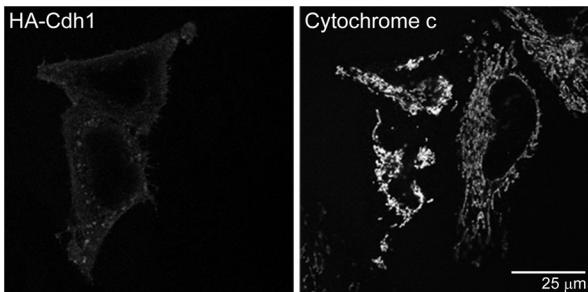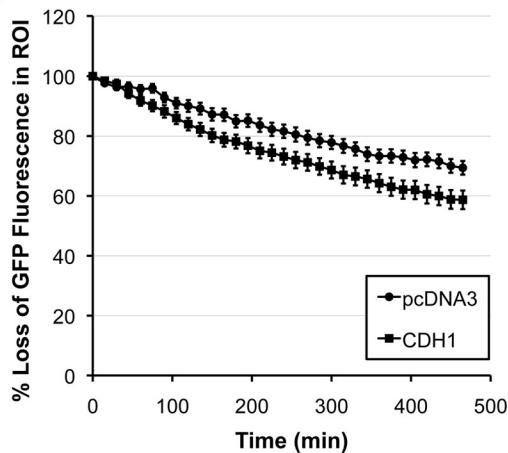
FIGURE 3: Cdh1-mediated changes in mitochondrial morphology. (A) Cytochrome *c* staining of mitochondrial morphology in asynchronous HeLa cells transfected with HA-Cdh1 (stained for HA, shown in green) or untransfected (no HA staining). Images shown are representative of multiple independent experiments. (B) HeLa cells were transfected with mito-PA-GFP and pCDNA3 or pCDNA3-HA-Cdh1. A small number of mitochondria per cell were illuminated with a UV laser (405 nM). The data represent the relative fluorescence of the UV-activated region of interest over time, and error bars represent the SE of the mean.

would be difficult to distinguish differences in degrees of mitochondrial fragmentation in cells overexpressing the WT Drp1 versus the Drp1 D-Box mutant (Labrousse *et al.*, 1999; Szabadkai *et al.*, 2004; Jagasia *et al.*, 2005). In other words, it seems that the APC/C is not sufficiently active against Drp1 to cope with overexpressed Drp1, leaving levels of Drp1 sufficient to induce mitochondrial fragmentation. Indeed, when we examined asynchronous cells that had been transfected with low levels of plasmid encoding either a Drp1 WT (FLAG)-tagged construct or a Drp1 D-Box mutant FLAG construct, we observed significant mitochondrial fragmentation with expression of both the WT and D-Box mutant constructs. When mitochondrial morphology was examined in early G1 cells, the expression of either construct (at approximately equal levels, based on quantification of FLAG fluorescence) resulted in a similar degree of mitochondrial fragmentation (Figure 4, D–F). To further examine any potential morphological differences between exogenous expression of either the Drp1 WT or the single D-Box mutant constructs, both FLAG fluorescence and the number of mitochondrial objects (based on cytochrome *c* fluorescence) were quantified for several individual WT and D-Box mutant-expressing cells. These data are shown in Figure 4, E and F (where each data point represents an individual cell). Together, these data demonstrate that, like the WT protein, the D-Box mutant protein is fully functional in inducing mitochondrial

fragmentation (in contrast to other known mutations within this domain of Drp1, which have a dominant-negative effect and actually block mitochondrial fission) (Waterham *et al.*, 2007).

We do consistently see increased expression of the D-Box mutant relative to the WT in overexpression experiments, and we see decreased ubiquitylation of the D-Box mutant, all consistent with an overall increase of the D-Box mutant protein relative to the WT. We believe, however, that expression of the WT protein (at levels comparable to the D-Box mutant protein) results in a comparable degree of mitochondrial fission. Thus the WT and D-Box mutants do not have inherently different biological activities. Rather, because they have different stabilities, and because mitochondrial fragmentation correlates with the levels of intracellular Drp1, phenotypic differences between WT and mutant proteins reflect their different abundance. Therefore, to further delineate the functional role of Cdh1-mediated Drp1 degradation, we wanted to investigate the effects of Cdh1-mediated Drp1 degradation in a Cdh1 loss-of-function context, as a more accurate way of addressing the physiological relevance of this degradation event.

Cdh1 regulates Drp1-dependent changes in mitochondrial morphology and metabolism during interphase

Consistent with a role for APC/C[Cdh1] in the degradation of Drp1, we detected elevated Drp1 protein levels in mouse embryonic fibroblasts (MEFs) generated from a Cdh1-null mouse, as has been reported for other Cdh1 substrates (Figure 5A) (Garcia-Higuera *et al.*, 2008; Li *et al.*, 2008). Moreover, when we immunoprecipitated Drp1 from either Cdh1 +/+ or –/– asynchronous MEF cell lysates, we noted a decrease in Drp1 ubiquitylation in the absence of Cdh1 (although some ubiquitylation still occurred, consistent with previous reports of other E3 ubiquitin ligases targeting Drp1) (Figure 5B) (Nakamura *et al.*, 2006; Yonashiro *et al.*, 2006; Karbowski *et al.*, 2007). We next compared levels of Drp1 protein during G1 phase in cell lysates generated from either the Cdh1^{+/+} MEFS versus the Cdh1^{–/–} MEFs, and we found that the amount of Drp1 protein remaining in the Cdh1^{–/–} cell lysates after release from nocodazole arrest was increased relative to the WT Cdh1^{+/+} MEF lysates (Figure 5C). Together, these data demonstrate that Drp1 ubiquitylation and degradation is decreased in the absence of Cdh1.

On the basis of our observation that overexpression of Cdh1 decreases Drp1 protein levels and promotes a more interconnected mitochondrial network, we wished to investigate the effects on mitochondrial morphology and function of an acute knockdown of Cdh1 in synchronized cells. Accordingly, we silenced Cdh1 expression, and then we examined mitochondrial morphology in a population of HeLa cells arrested at the G1/S border. During this point in the cell cycle, mitochondria normally form an elongated network, as we saw in our scrambled control RNAi. RNAi-mediated silencing of Cdh1 resulted in the predominance of short, punctate mitochondria (Figure 6A, top panels). This mitochondrial fragmentation induced by Cdh1 RNAi was dependent on Drp1, as knocking down both Cdh1 and Drp1 attenuated this effect (Figure 6A, bottom panels; quantified in Figure 6B).

On the basis of the recent report from Lippincott-Schwartz and colleagues that a hyperfused mitochondrial state at G1/S regulates cyclin E accumulation, we tested whether the acute knockdown of Cdh1 (and the resulting mitochondrial fragmentation) would consequently decrease levels of cyclin E (Mitra *et al.*, 2009). Indeed, we saw a decrease in cyclin E levels in Cdh1-RNAi cells relative to RNAi control cells both in early G1 cells (Figure 6C) and in cells arrested at G1/S (unpublished data). Importantly, this decrease was attenuated in the presence of the double Cdh1/Drp1 knockdown, suggesting
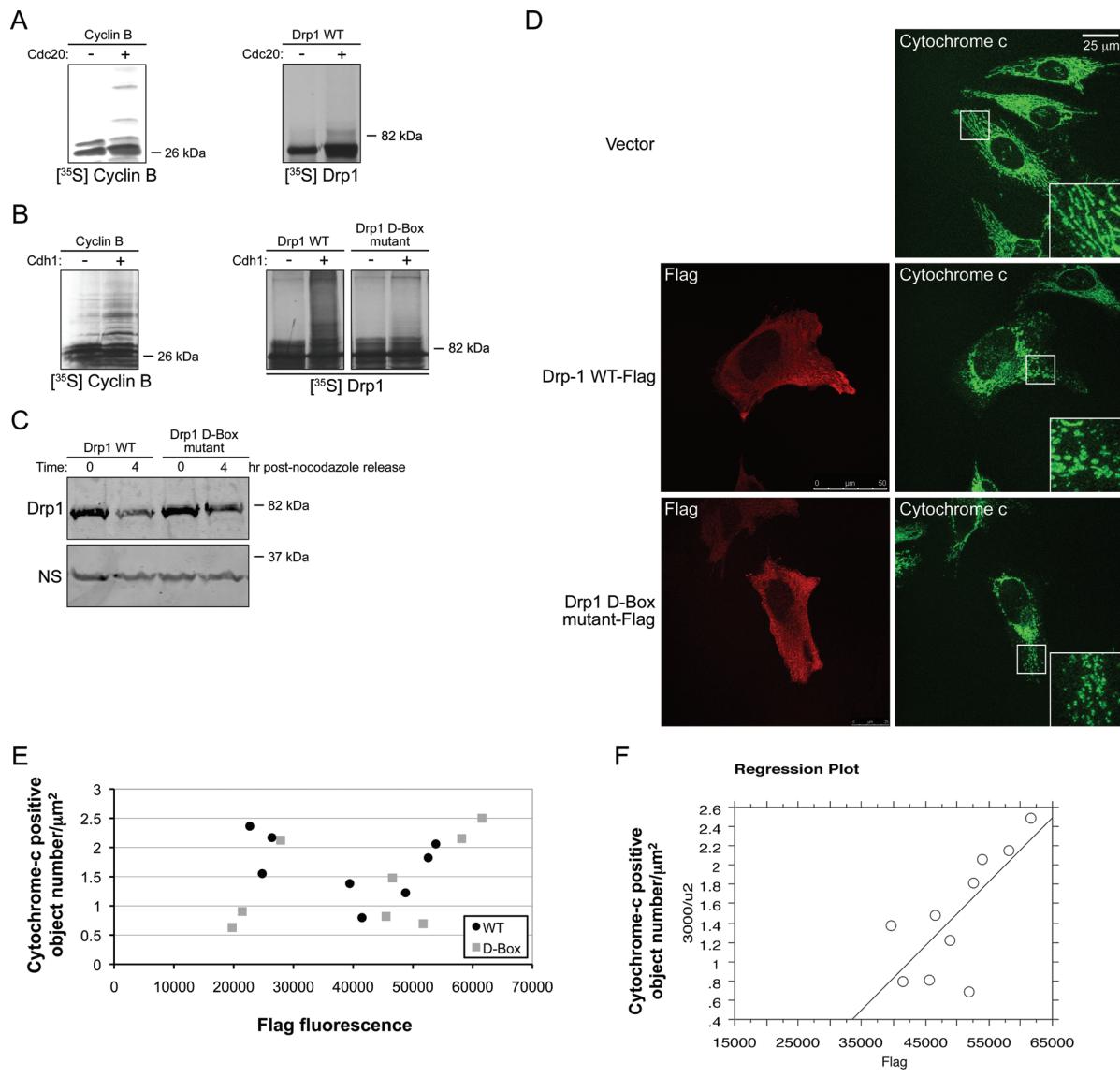
FIGURE 4: Requirements for APC/C[Cdh1]-mediated degradation of Drp1. (A) Ubiquitylation of in vitro–translated [35S]-Drp1 by immunopurified APC/C supplemented with recombinant Cdc20 (A) or Cdh1 (B). An N-terminal fragment of Cyclin B1 is shown as a positive control. (C) HeLa lysates expressing either Drp1 WT or Drp1 D-Box mutant at the indicated times after release from nocodazole arrest. A nonspecific band (NS) of ~30 kDa is shown as a loading reference. When normalized for loading, there is an 11% increase in the Drp1 D-Box mutant relative to the WT construct. (D) FLAG and cytochrome *c* staining of mitochondrial morphology in a HeLa cells transfected with either FLAG-tagged pcDNA3-Drp1 WT or Flag-tagged pcDNA3-Drp1 D-Box mutant (vs. untransfected cells, showing no Flag staining in top panel). The maximum projection of z-stacks is shown for cytochrome *c* immunofluorescence. (E) Images were acquired and analyzed using exactly the same parameters (gain and offset values were the same), to allow for comparisons between image sets from the same experiment. Both FLAG fluorescence and the number of mitochondrial objects (based on cytochrome *c* fluorescence) were quantified for several individual WT and D-Box mutant-expressing cells, and each data point in the graph represents an individual cell. Two populations of FLAG-positive cells emerged during our analysis: a population with relative FLAG-fluorescence less than 30,000 U, and a population with fluorescence greater than 40,000 relative units. For the population with lower FLAG fluorescence, the expression of either construct did not correlate with the degree of mitochondrial fragmentation, whereas it did for the second population. The lack of correlation in the first population could reflect: decreased APC/C[Cdh1] activity in that subset of cells, decreased mitochondrial fusion to oppose Drp1-dependent fission, or a lack of tight synchronization in early G1 (for instance, that population of cells could be earlier in the process of mitotic exit, thus showing mitotic fragmentation that is independent of the exogenous Drp1). (F) Linear regression analysis of cells expressing FLAG-tagged pcDNA3-Drp1 WT or FLAG-tagged pcDNA3-Drp1 D-box mutant constructs (from the second population, with fluorescence greater than 40,000 relative units). The y-axis shows fluorescence and mitochondrial object number per unit area, and the x-axis shows relative FLAG fluorescence. For this population of cells, the expression of both FLAG-Drp1 and FLAG-D-Box mutant Drp1 was correlated with increased mitochondrial object number (r = 0.74; r^2 = 0.544; p = 0.02), although there was no significant difference in the degree of mitochondrial fragmentation caused by the two constructs (the WT vs. D-Box mutant).
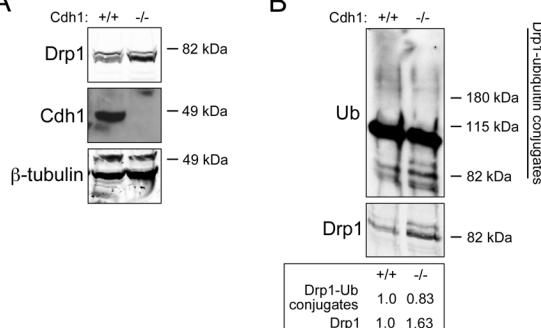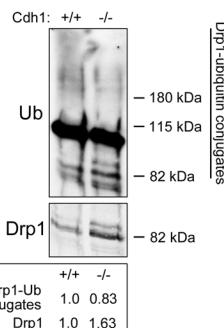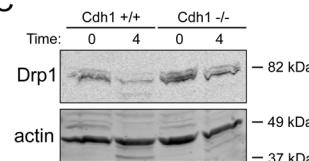
FIGURE 5: Cdh1 regulates Drp1 abundance. (A) Immunodetection of Cdh1 and Drp1 in lysates prepared from proliferating WT or Cdh1-null MEFs. β-tubulin is shown as a loading control. (B) Drp1 immunoprecipitates generated from WT or Cdh1-null MEFs were immunoblotted for ubiquitin. The relative abundance of Drp1-ubiquitin conjugates and Drp1 protein levels is shown. (C) Lysates were prepared from either WT or Cdh1-null MEFS at the indicated times after release from nocodazole arrest and were immunoblotted for Drp1.

that the changes in mitochondrial morphology resulting from Cdh1-mediated Drp1 degradation correlated with cyclin E levels.

We next wanted to determine whether cellular metabolism was affected by mitochondrial fragmentation induced by the knockdown of Cdh1. Despite undetectable changes in cellular ATP levels in any of the cell types tested (Supplemental Figure 2), more detailed analysis revealed distinct changes in mitochondrial metabolism. Using a metabolomics approach, we analyzed steady-state levels of acyl-carnitines, metabolites that can be derived from several sources including glucose, amino acids, and lipids and reflect the mitochondrial acyl-CoA pool. The acute knockdown of Cdh1 in a G1/S-arrested HeLa cell population
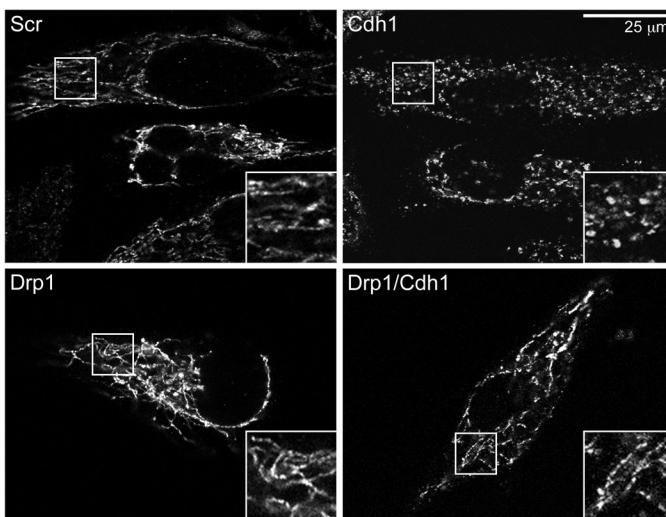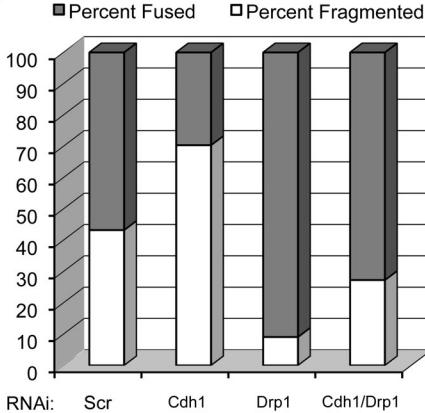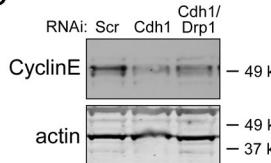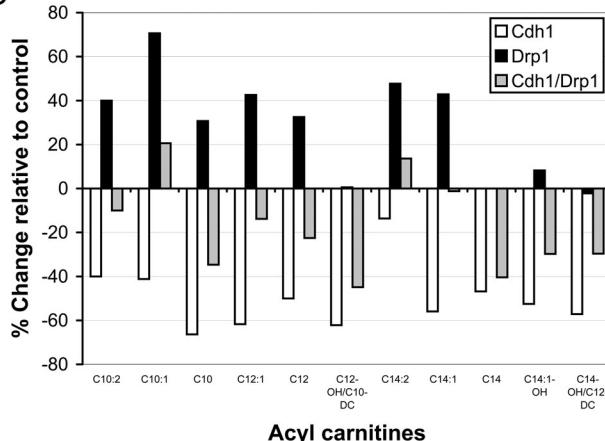
FIGURE 6: Cdh1 regulates Drp1-dependent changes in mitochondrial morphology and metabolism during interphase. (A) Cytochrome c staining of mitochondrial morphology in G1/S-arrested cells transfected with the following siRNA oligonucleotides: Scrambled, Cdh1, Drp1, and both Drp1 and Cdh1. Images shown are representative of multiple independent experiments. (B) Blind quantification of (A) (n = 4). (C) Cyclin E immunoblotting in siRNA-transfected, early-G1-phase HeLa cells. (D) MS/MS-based analysis of acyl-carnitine species in G1/S-arrested HeLa cells transfected with the indicated siRNAs. Means of triplicate samples are shown as percent change relative to the scrambled RNAi control.

drastically altered the steady-state levels of acyl-carnitines. Specifically, in the absence of Cdh1, there was a dramatic decrease in the abundance of most medium-chain acyl-carnitines and several long chain acyl-carnitines (unpublished observations), a profile that is consistent with a block in fatty acid β-oxidation. Many of these changes were attenuated by dual knock-down of Drp1 and Cdh1, suggesting that the β-oxidation defects produced by loss of Cdh1 correlated with Cdh1-mediated changes in Drp1 levels (Figure 6D). For a number of the metabolites measured, loss of Drp1 alone produced changes in levels opposite to loss of Cdh1, again suggesting that perturbation of Drp1 levels, with consequent alterations in mitochondrial morphology, could have marked effects on cellular metabolism.

DISCUSSION

Based on the results just mentioned, APC/C^{Cdh1}-mediated degradation of Drp1 appeared to underlie the morphological changes occurring in the mitochondria following cell division. It has been suggested that the transition from an interconnected mitochondrial network during interphase to a fragmented morphology during mitosis not only might function to physically separate mitochondria into daughter cells, but also might reflect variations in energy needs and utilization during the cell cycle (Benard and Rossignol, 2008; Grandemange et al., 2009). The recent identification of retrograde signaling pathways from the mitochondria has uncovered a metabolic checkpoint at the G1/S boundary, highlighting the importance of ensuring that cellular proliferation is coordinated with sufficient metabolic capacity and proper mitochondrial function (Jones et al., 2005; Mandal et al., 2005, 2010; Owusu-Ansah et al., 2008; Mitra et al., 2009).

Although the relationships between morphology and mitochondrial metabolism are not fully understood, the decrease in levels of Drp1 protein temporally coincided with the return of mitochondria to a reticular morphology and with the significant increases in membrane potential and respiration that occur during progression through G1 (Schieke et al., 2008). A hyperfused mitochondrial state at G1/S is necessary for cyclin E accumulation and cell-cycle progression, and Drp1-dependent mitochondrial fragmentation induced by overexpression of the novel mitochondrial inner-membrane protein MTGM halts cells in the S phase of the cell cycle (Mitra et al., 2009; Zhao et al., 2009). Thus we hypothesize that APC/C^{Cdh1}-mediated degradation of Drp1 (and the resulting reestablishment of the mitochondrial network) might function to serve the metabolic demands of a proliferating cell.

Although we did not observe delays in cell-cycle progression due to alterations in mitochondrial morphology during our limited time course, it is quite possible that the increased mitochondrial fragmentation we observed (due to loss of Cdh1) might have cumulative effects following several cell divisions. The persistently fragmented mitochondrial morphology that results in the absence of Cdh1-mediated Drp1 degradation (and the subsequent decreases in cyclin E and alterations in lipid-derived metabolites) may have cumulative deleterious effects on mitochondrial function, comparable to the severe defects in cell growth, mitochondrial membrane potential, and cellular respiration observed in cells deficient in the mitochondrial fusion proteins Mfn1 and Mfn2 (which display fragmented mitochondria due to a complete lack of mitochondrial fusion) (Chen et al., 2005).

Mitochondrial defects, such as those occurring in obesity and insulin resistance, are associated with decreased Mfn2 expression and mitochondrial network formation (Zorzano, 2009). Inhibition of Drp1-induced mitochondrial fission has been shown to ameliorate high glucose–mediated cell death (Yu et al., 2006), and a recently reported mutation in Drp1 resulted in lethality marked by microcephaly and metabolic aberrations (Waterham et al., 2007). In mouse models, cells deficient in both Mfn1 and Mfn2 display fragmented mitochondria due to a complete lack of mitochondrial fusion and show severe defects in cell growth, mitochondrial membrane potential, and cellular respiration (Chen et al., 2003, 2005). Given these and other links between alterations in the mitochondrial fission/fusion balance and perturbations in cellular metabolism, it is interesting to note that both the Mfn2-deficient and Cdh1-deficient mice display similar deficiencies in both cell size and number in giant cells of the placental trophoblast (Chen et al., 2003; Garcia-Higuera et al., 2008; Li et al., 2008). It is therefore possible that unbalanced mitochondrial fragmentation contributes to placental abnormality in both of these lethal phenotypes.

Our finding that inhibition of Cdh1-mediated degradation of Drp1 during interphase prevents cyclin E accumulation and alters the profile of lipid-derived metabolites is part of growing evidence of a link between cellular proliferation and mitochondrial metabolism. Evidence from multiple research groups suggests a "metabolic checkpoint" at the G1/S boundary in which several signaling pathways (including AMP-activated protein kinase–induced p53 activation as well as reactive oxygen species–mediated up-regulation of a fly cyclin-dependent kinase inhibitor homologue) converge to modulate cyclin E levels and activity (Jones et al., 2005; Mandal et al., 2005, 2010; Owusu-Ansah et al., 2008; Mitra et al., 2009). Specifically, through its degradation of target proteins, the APC/C^{Cdh1} complex is emerging as an important link between the regulation of cell proliferation and bioenergetic status (Almeida et al., 2009; Herrero-Mendez et al., 2009; Colombo et al., 2010). The cross-talk between regulators of mitochondrial dynamics and key cell-cycle regulators may ensure that mitochondrial function is tightly linked to cell growth and proliferation. Together, these data highlight an exciting new area of research on the contribution of mitochondrial metabolism and network status to cell-cycle progression.

Through the degradation of substrates such as the Skp1/Cullin/F-box protein (SCF) component Skp2 and the inhibitor of DNA replication geminin, the APC/C^{Cdh1} complex regulates the proper timing of G1 and S phases. Here we describe a novel role for APC/C^{Cdh1} in the degradation of the mitochondrial fission protein Drp1. APC/C^{Cdh1}-mediated Drp1 degradation is important for maintaining mitochondrial network formation and metabolic function during interphase, suggesting that the APC/C^{Cdh1} complex may also regulate the distinct bioenergetic needs of a growing cell during synthetic phases of the cell cycle.

MATERIALS AND METHODS

Plasmids and protein expression

Hemagglutinin (HA)-tagged Cdh1 and Cdc20 plasmids were a gift from M. Pagano (New York University, New York, NY). The Drp1 expression construct was provided by A.M. van der Bliek (University of California, Los Angeles, CA), and was subcloned into pcDNA3 with a C-terminal FLAG tag. For protein production, Drp1 was first subcloned into the pENTR-3C vector (Invitrogen, Carlsbad, CA) and then recombined into pDEST17 using LR Clonase II (Invitrogen). Recombinant Cdh1 protein was a gift from the Ronai Lab (Sanford-Burnham Institute for Medical Research, La Jolla, CA). The Drp1 D-Box mutant was prepared with a QuikChange Site-Directed Mutagenesis Kit (Stratagene, La Jolla, CA) using the following primer sequence: 5′-gtg act tgt ctt ctt gcc aaa agg gcc cct gtt aca aat g -3′.

Antibodies

The primary antibodies used for immunoblotting, immunoprecipitations, and immunofluorescence were as follows: anti-Drp1 (BD

Transduction Laboratories, Franklin Lakes, NJ); Phospho-Histone H3 (Cell Signaling Technology, Danvers, MA); anti-actin, anti-HA, anti-Cdc27, anti-Cyclin E, and Cyclin B1 (monoclonal and polyclonal) (Santa Cruz Biotechnology, Santa Cruz, CA); anti-Cdh1 (Thermo Scientific, Kalamazoo, MI); anti-FLAG (polyclonal; Sigma, St. Louis, MO); and anti-cytochrome *c* (BD PharMingen, Sparks, MD). The Mfn2 antibody was a gift from Richard Youle (National Institute of Neurological Disorders and Stroke, Bethesda, MD). AlexaFluor (Invitrogen) and IR-Dye (LI-COR Biosciences, Lincoln, NE) secondary antibodies were used for immunofluorescence or for immunoblotting with the LI-COR Imaging System, or horseradish peroxidase–conjugated antibodies (from Promega, Madison, WI, and Dako, Carpenteria, CA) were used with an ECL-Plus detection system (Amersham Biosciences, Piscataway, NJ).

For immunofluorescence, cells were stained with the following primary antibodies: anti-FLAG (Sigma), anti-HA (Santa Cruz Biotechnology), or anti-cytochrome *c* (BD PharMingen). Following phosphate-buffered saline (PBS) washes, cells were next incubated with secondary antibodies, including goat anti–rabbit Alexa 488, goat anti–mouse Alexa 594, or goat anti–rabbit Alexa 561 (Molecular Probes, Eugene, OR, or Invitrogen).

Cell culture and synchronization
HeLa, HeLa S3, and HEK 293T cells were grown in DMEM with 10% fetal bovine serum (FBS). For double thymidine block experiments, HeLa and HeLa S3 cells were synchronized by sequential incubations with 2.5 mM thymidine and either released into medium containing nocodazole at 40 ng/ml (for G1/S release experiments) or analyzed during the second thymidine block (for mitochondrial morphology and metabolomics). To generate early G1 cells for immunofluorescence, cells were examined 14.5–16 h following release from the second thymidine arrest. For nocodazole release experiments, HeLa and HeLa S3 cells were blocked in medium containing nocodazole 40 ng/ml for 16–17 h. Nonadherent cells were washed three times in PBS and released into complete medium. At the indicated times after release, adherent cells were harvested for Western blotting. For nocodazole release experiments in Cdh1 MEFS, cells were synchronized using a single thymidine block (2.5 mM) and were then released into medium containing nocodazole at 80 ng/ml for 17 h. Cells were released and harvested as described earlier in text. In vitro mitotic exit assays were performed as previously described (Wu *et al.*, 2009). For Western blotting, cells were lysed in cold RIPA buffer (50 mM Tris, pH 7.4, 1% Nonidet P-40 [NP-40], 0.25% sodium deoxycholate, 1 mM EDTA, 0.1% SDS, 150 mM NaCl supplemented with aprotonin and leupeptin at 10 µg/ml, and 1 mM sodium vanadate). Lysate concentrations were determined by Bradford assay (Bio-Rad, Hercules, CA), and concentrations were normalized before loading onto SDS–PAGE gels. Proteasome inhibitors were used at the following concentrations: lactacystin (Sigma, St. Louis, MO) at 30 µM for 6 h; MG132 (Calbiochem, San Diego, CA) at 20 µM for 5 h or epoxomicin (Calbiochem) at 2.5 µM for 11 h.

Cdh1 WT and null MEFS were provided by the Malumbres Lab (The Spanish National Cancer Research Center [CNIO], Madrid), and were cultured in DMEM supplemented with 10% FBS and 2 mM L-glutamine.

In vitro APC assay
The APC assay was performed as previously described (Wu *et al.*, 2007) with the following modifications: immunoprecipitated *Xenopus* APC was incubated with either Cdc20 or Cdh1 at room temperature for 1 h, and then ^{35}S-labeled human Drp1 was added in the presence of recombinant E1, E2, and ATP.

Transfections
Plasmid transfections were performed using Fugene 6 (Roche, Basel, Switzerland), according to the manufacturer's instructions. siRNA oligonucleotides were transfected using Lipofectamine RNAiMAX (Invitrogen), according to the manufacturer's instructions. For RNAi transfection/synchronization experiments, HeLa cells were plated at subconfluent densities and were transfected twice with siRNA constructs, before both the first and second thymidine block.

siRNA
siRNAs were purchased from Dharmacon (Lafayette, CO). A nontargeting siRNA was used as a negative control (siGENOME siRNA #2), an ON-TARGET plus SMARTpool was used for Drp1, and the Cdh1 siRNA nucleotide sequence has been described previously (Bashir *et al.*, 2004). To quantify changes in mitochondrial morphology for siRNA-transfected cells, the individual initially acquiring the images had been blinded as to with which RNAi oligonucleotides the cells had been transfected. Next all of the previously acquired images (for four total assay trials) were assigned random letters, and the mitochondria in each cell in the image were scored as fragmented, fused, or not able to be scored by another individual.

Immunoprecipitations
HEK 293T cells were lysed with IP buffer (50 mM Tris, pH 7.5, 150 mM NaCl, 1% NP-40, 0.5% sodium deoxycholate, and Complete Protease Inhibitor [Roche]), and extracts were incubated with HA antibody (3 µg) for 1 h at 4°C before Protein A Sepharose was added. Immunoprecipitates were washed three times in IP buffer before loading onto SDS–PAGE gels for immunoblotting.

For Drp1-ubiquitylation experiments, WT or Cdh1 null MEFS were pretreated with 20 µM MG132 for 6 h prior to lysis in IP buffer. Lysates were quantitated by Bradford assay (Bio-Rad), and protein concentrations were normalized prior to incubation with Drp1-conjugated Protein G Sepharose for 2 h at 4°C. Immunoprecipitates were washed three times in IP buffer prior to SDS–PAGE and immunoblotting.

Preparation of recombinant proteins and pulldowns
pDEST17-Drp1 was generated from pENTR-3C-Drp1, according to the manufacturer's instructions (Invitrogen). pDEST17-Drp1 was then transformed into BL21-AI cells (Invitrogen), and His-Drp1 was purified using Ni-affinity chromatography (Ni-NTA agarose; Qiagen, Germantown, MD). Ni-bound His-Drp1 beads were washed first in wash buffer containing 10 mM HEPES, pH 7.5, 500 mM NaCl with 0.02% Triton X-100 and then in wash buffer without Triton X-100. Control nickel beards were preblocked in 0.125 M histidine. Both sets of bead (control nickel and Ni-bound His-Drp1) were washed in IP buffer and then incubated with cell lysates (lysed in IP buffer) for 2 h at 4°C. The beads were washed three times in IP buffer before being loaded onto SDS–PAGE gels for immunoblotting. MBP and MBP-Emi2 were produced as previously described (Wu *et al.*, 2007), except that amylose resin (New England Niolabs, Ipswich, MA) was used and proteins were eluted with 20 mM maltose.

Immunofluorescence and microscopy
On the basis of our observations of mitochondrial morphology in HeLa cells exiting mitosis, we noted a discrepancy in the timing of mitochondrial elongation and network establishment between cells exiting release from a nocodazole arrest and cells that had been arrested at the G1/S border and allowed to progress through mitosis in absence of nocodazole. Specifically, nocodazole-arrested cells

did not show mitochondrial network formation until 6 h following release, whereas reformation of the network occurred quickly during mitotic exit in our experiments using unperturbed live cells, consistent with previous reports. This discrepancy can likely be attributed to the importance of microtubules in maintaining mitochondrial morphology (Frederick and Shaw, 2007). Thus, for synchronized cell experiments, we examined mitochondrial morphology either at the G1/S boundary or 14.5 h following release from double thymidine arrest (early G1).

Cells were fixed in 4% formaldehyde for 10 min, permeabilized with 0.5% Triton X-100 for 5 min, and then blocked with 5% goat serum before immunostaining. Mitochondrial morphology was analyzed using an Olympus (Center Valley, PA) IX-70 spinning disk confocal or a Leica (Buffalo Grove, IL) SP5 confocal microscope. For the spinning disk confocal, the 100×/1.35 oil objective was used with 488-nm laser lines for excitation with an Hamamatsu (Hamamatsu City, Japan) ORCA ER CCD camera, and the system was controlled by MetaMorph (Molecular Devices, Sunnyvale, CA). For the Leica SP5 confocal, the 100×/1.4 oil objective was used with 488-, 561-, and 594-nm laser lines for excitation.

For determination of FLAG fluorescence and mitochondrial object numbers, early G1 cells (fixed at 14.5 h following release from a double thymidine block) were imaged using a Leica SP5 confocal microscope. The images were acquired using the same parameters (100×/1.4 oil immersion objective with 488- and 561-nm laser lines for excitation, with the same gain and offset values used for each image) to allow for comparison of images. Image deconvolution was performed using Huygens Essential software (Scientific Volume Imaging, Hilversum, The Netherlands), using the batch processor with a signal-to-noise ratio of 8 and a maximum of 40 iterations. The output was 16-bit, unscaled images to allow the comparison of pixel values across images (as described in Howell et al., 2009). Cytochrome c–positive objects were analyzed using the same threshold values (to control for background), using the Huygens Object Analyzer program. For quantification of FLAG fluorescence, maximum projection of all the z-stacks was generated using Leica Microsystems LAS AF Software. Cellular area was determined using MetaMorph software, and values are shown as the number of cytochrome c–positive objects per unit area.

To measure mitochondrial fusion using the diffusion of photoactivatable mito-GFP following photoactivation, HeLa cells were transfected with mito-PA-GFP and pCDNA3 or pCDNA3-HA-CDH1 at a 1:6 μg ratio (mito-PA-GFP:pCDNA3) for 18 h using Fugene 6 (Roche) in 30-mm coverslip dishes (MatTek, Ashland, MA). Cell medium was supplemented with 25 mM HEPES, pH 7.4. The cells were then visualized on a Leica SP5 confocal microscope at 37°C. A small number of mitochondria per cell were illuminated with a UV laser (405 nM) for 3 s. Images were then taken every 15 s for 8 min. The data represent the relative fluorescence of the UV-activated region of interest over time. The data are presented as a percentage of the fluorescence at time zero. Each data point represents averaged relative fluorescence measurements at each time point from at least 75 regions of interest from transfected cells. Error bars represent the SE of the mean.

Acyl-carnitine and metabolic analysis

HeLa cells that had been transfected with siRNA were incubated with 1 μM L-carnitine for 20–22 h during the final thymidine block. Sterile water was added to harvested cell pellets, and cells were lysed by sonication. Protein concentrations were determined by Bradford assay (Bio-Rad), and triplicate samples were prepared (with normalized protein concentrations) for targeted analysis of acyl-carnitine levels by tandem mass spectrometry (MS/MS) as previously described (An et al., 2004; Newgard et al., 2009).

ATP assay

ATP levels in siRNA-transfected HeLa cells, arrested at the G1/S boundary, are shown in the Supplemental Materials and Methods. Equal cells numbers were harvested following the second thymidine incubation, and relative bioluminescence was measured for triplicate samples using the ATP Bioluminescence Assay Kit CLS II (Roche).

REFERENCES

Almeida A, Bolanos JP, Moncada S (2009). E3 ubiquitin ligase APC/C-Cdh1 accounts for the Warburg effect by linking glycolysis to cell proliferation. Proc Natl Acad Sci USA 107, 738–741.

Amiott EA, Cohen MM, Saint-Georges Y, Weissman AM, Shaw JM (2009). A mutation associated with CMT2A neuropathy causes defects in Fzo1 GTP hydrolysis, ubiquitylation, and protein turnover. Mol Biol Cell 20, 5026–5035.

An J, Muoio DM, Shiota M, Fujimoto Y, Cline GW, Shulman GI, Koves TR, Stevens R, Millington D, Newgard CB (2004). Hepatic expression of malonyl-CoA decarboxylase reverses muscle, liver and whole-animal insulin resistance. Nat Med 10, 268–274.

Araki M, Yu H, Asano M (2005). A novel motif governs APC-dependent degradation of Drosophila ORC1 in vivo. Genes Dev 19, 2458–2465.

Barni S, Sciola L, Spano A, Pippia P (1996). Static cytofluorometry and fluorescence morphology of mitochondria and DNA in proliferating fibroblasts. Biotech Histochem 71, 66–70.

Bashir T, Dorrello NV, Amador V, Guardavaccaro D, Pagano M (2004). Control of the SCF(Skp2-Cks1) ubiquitin ligase by the APC/C(Cdh1) ubiquitin ligase. Nature 428, 190–193.

Bassermann F, Frescas D, Guardavaccaro D, Busino L, Peschiaroli A, Pagano M (2008). The Cdc14B-Cdh1-Plk1 axis controls the G2 DNA-damage-response checkpoint. Cell 134, 256–267.

Benard G, Karbowski M (2009). Mitochondrial fusion and division: Regulation and role in cell viability. Semin Cell Dev Biol 20, 365–374.

Benard G, Rossignol R (2008). Ultrastructure of the mitochondrion and its bearing on function and bioenergetics. Antioxid Redox Signal 10, 1313–1342.

Castro A, Vigneron S, Bernis C, Labbe JC, Lorca T (2003). Xkid is degraded in a D-box, KEN-box, and A-box-independent pathway. Mol Cell Biol 23, 4126–4138.

Chang CR, Blackstone C (2007). Cyclic AMP-dependent protein kinase phosphorylation of Drp1 regulates its GTPase activity and mitochondrial morphology. J Biol Chem 282, 21583–21587.

Chen H, Chomyn A, Chan DC (2005). Disruption of fusion results in mitochondrial heterogeneity and dysfunction. J Biol Chem 280, 26185–26192.

Chen H, Detmer SA, Ewald AJ, Griffin EE, Fraser SE, Chan DC (2003). Mitofusins Mfn1 and Mfn2 coordinately regulate mitochondrial fusion and are essential for embryonic development. J Cell Biol 160, 189–200.

Cho DH, Nakamura T, Fang J, Cieplak P, Godzik A, Gu Z, Lipton SA (2009). S-nitrosylation of Drp1 mediates beta-amyloid-related mitochondrial fission and neuronal injury. Science 324, 102–105.

Colombo SL, Palacios-Callender M, Frakich N, De Leon J, Schmitt CA, Boorn L, Davis N, Moncada S (2010). Anaphase-promoting complex/cyclosome-Cdh1 coordinates glycolysis and glutaminolysis with transition to S phase in human T lymphocytes. Proc Natl Acad Sci USA 107, 18868–18873.

Crane R, Kloepfer A, Ruderman JV (2004). Requirements for the destruction of human Aurora-A. J Cell Sci 117, 5975–5983.

Cribbs JT, Strack S (2007). Reversible phosphorylation of Drp1 by cyclic AMP-dependent protein kinase and calcineurin regulates mitochondrial fission and cell death. EMBO Rep 8, 939–944.

Escobar-Henriques M, Westermann B, Langer T (2006). Regulation of mitochondrial fusion by the F-box protein Mdm30 involves proteasome-independent turnover of Fzo1. J Cell Biol 173, 645–650.

Frederick RL, Shaw JM (2007). Moving mitochondria: establishing distribution of an essential organelle. Traffic 8, 1668–1675.

Fritz S, Weinbach N, Westermann B (2003). Mdm30 is an F-box protein required for maintenance of fusion-competent mitochondria in yeast. Mol Biol Cell 14, 2303–2313.

Garcia-Higuera I, Manchado E, Dubus P, Canamero M, Mendez J, Moreno S, Malumbres M (2008). Genomic stability and tumour suppression by the APC/C cofactor Cdh1. Nat Cell Biol 10, 802–811.

Grandemange S, Herzig S, Martinou JC (2009). Mitochondrial dynamics and cancer. Semin Cancer Biol 19, 50–56.

Han XJ, Lu YF, Li SA, Kaitsuka T, Sato Y, Tomizawa K, Nairn AC, Takei K, Matsui H, Matsushita M (2008). CaM kinase I alpha-induced phosphorylation of Drp1 regulates mitochondrial morphology. J Cell Biol 182, 573–585.

Harder Z, Zunino R, McBride H (2004). Sumo1 conjugates mitochondrial substrates and participates in mitochondrial fission. Curr Biol 14, 340–345.

Herrero-Mendez A, Almeida A, Fernandez E, Maestre C, Moncada S, Bolanos JP (2009). The bioenergetic and antioxidant status of neurons is controlled by continuous degradation of a key glycolytic enzyme by APC/C-Cdh1. Nat Cell Biol 11, 747–752.

Howell AS, Savage NS, Johnson SA, Bose I, Wagner AW, Zyla TR, Nijhout HF, Reed MC, Goryachev AB, Lew DJ (2009). Singularity in polarization: rewiring yeast cells to make two buds. Cell 139, 731–743.

Ishihara N et al. (2009). Mitochondrial fission factor Drp1 is essential for embryonic development and synapse formation in mice. Nat Cell Biol 11, 958–966.

Jagasia R, Grote P, Westermann B, Conradt B (2005). DRP-1-mediated mitochondrial fragmentation during EGL-1-induced cell death in Celegans. Nature 433, 754–760.

Jones RG, Plas DR, Kubek S, Buzzai M, Mu J, Xu Y, Birnbaum MJ, Thompson CB (2005). AMP-activated protein kinase induces a p53-dependent metabolic checkpoint. Mol Cell 18, 283–293.

Karbowski M, Neutzner A, Youle RJ (2007). The mitochondrial E3 ubiquitin ligase MARCH5 is required for Drp1 dependent mitochondrial division. J Cell Biol 178, 71–84.

Labrousse AM, Zappaterra MD, Rube DA, Van Der Bliek AM (1999). Celegans dynamin-related protein DRP-1 controls severing of the mitochondrial outer membrane. Mol Cell 4, 815–826.

Li M, Shin YH, Hou L, Huang X, Wei Z, Klann E, Zhang P (2008). The adaptor protein of the anaphase promoting complex Cdh1 is essential in maintaining replicative lifespan and in learning and memory. Nat Cell Biol 10, 1083–1089.

Mandal S, Freije WA, Guptan P, Banerjee U (2010). Metabolic control of G1-S transition: cyclin E degradation by p53-induced activation of the ubiquitin-proteasome system. J Cell Biol 188, 473–479.

Mandal S, Guptan P, Owusu-Ansah E, Banerjee U (2005). Mitochondrial regulation of cell cycle progression during development as revealed by the tenured mutation in Drosophila. Dev Cell 9, 843–854.

Margineantu DH, Gregory Cox W, Sundell L, Sherwood SW, Beechem JM, Capaldi RA (2002). Cell cycle dependent morphology changes and associated mitochondrial DNA redistribution in mitochondria of human cell lines. Mitochondrion 1, 425–435.

Mitra K, Wunder C, Roysam B, Lin G, Lippincott-Schwartz J (2009). A hyperfused mitochondrial state achieved at G1-S regulates cyclin E buildup and entry into S phase. Proc Natl Acad Sci USA 106, 11960–11965.

Nakamura N, Kimura Y, Tokuda M, Honda S, Hirose S (2006). MARCH-V is a novel mitofusin 2- and Drp1-binding protein able to change mitochondrial morphology. EMBO Rep 7, 1019–1022.

Neutzner A, Benard G, Youle RJ, Karbowski M (2008). Role of the ubiquitin conjugation system in the maintenance of mitochondrial homeostasis. Ann N Y Acad Sci 1147, 242–253.

Newgard CB et al. (2009). A branched-chain amino acid-related metabolic signature that differentiates obese and lean humans and contributes to insulin resistance. Cell Metab 9, 311–326.

Okamoto K, Shaw JM (2005). Mitochondrial morphology and dynamics in yeast and multicellular eukaryotes. Annu Rev Genet 39, 503–536.

Owusu-Ansah E, Yavari A, Mandal S, Banerjee U (2008). Distinct mitochondrial retrograde signals control the G1-S cell cycle checkpoint. Nat Genet 40, 356–361.

Park YY, Lee S, Karbowski M, Neutzner A, Youle RJ, Cho H (2010). Loss of MARCH5 mitochondrial E3 ubiquitin ligase induces cellular senescence through dynamin-related protein 1 and mitofusin 1. J Cell Sci 123, 619–626.

Schieke SM, McCoy JP Jr, Finkel T (2008). Coordination of mitochondrial bioenergetics with G1 phase cell cycle progression. Cell Cycle 7, 1782–1787.

Szabadkai G, Simoni AM, Chami M, Wieckowski MR, Youle RJ, Rizzuto R (2004). Drp-1-dependent division of the mitochondrial network blocks intraorganellar Ca2+ waves and protects against Ca2+-mediated apoptosis. Mol Cell 16, 59–68.

Taguchi N, Ishihara N, Jofuku A, Oka T, Mihara K (2007). Mitotic phosphorylation of dynamin-related GTPase Drp1 participates in mitochondrial fission. J Biol Chem 282, 11521–11529.

Wasiak S, Zunino R, McBride HM (2007). Bax/Bak promote sumoylation of DRP1 and its stable association with mitochondria during apoptotic cell death. J Cell Biol 177, 439–450.

Waterham HR, Koster J, van Roermund CW, Mooyer PA, Wanders RJ, Leonard JV (2007). A lethal defect of mitochondrial and peroxisomal fission. N Engl J Med 356, 1736–1741.

Wu JQ, Guo JY, Tang W, Yang CS, Freel CD, Chen C, Nairn AC, Kornbluth S (2009). PP1-mediated dephosphorylation of phosphoproteins at mitotic exit is controlled by inhibitor-1 and PP1 phosphorylation. Nat Cell Biol 11, 644–651.

Wu Q et al. (2007). A role for Cdc2- and PP2A-mediated regulation of Emi2 in the maintenance of CSF arrest. Curr Biol 17, 213–224.

Yonashiro R et al. (2006). A novel mitochondrial ubiquitin ligase plays a critical role in mitochondrial dynamics. EMBO J 25, 3618–3626.

Yu T, Robotham JL, Yoon Y (2006). Increased production of reactive oxygen species in hyperglycemic conditions requires dynamic change of mitochondrial morphology. Proc Natl Acad Sci USA 103, 2653–2658.

Zhao J, Liu T, Jin SB, Tomilin N, Castro J, Shupliakov O, Lendahl U, Nister M (2009). The novel conserved mitochondrial inner-membrane protein MTGM regulates mitochondrial morphology and cell proliferation. J Cell Sci 122, 2252–2262.

Zorzano A (2009). Regulation of mitofusin-2 expression in skeletal muscle. Appl Physiol Nutr Metab 34, 433–439.

Zunino R, Braschi E, Xu L, McBride HM (2009). Translocation of SenP5 from the nucleoli to the mitochondria modulates DRP1 dependent fission during mitosis. J Biol Chem 284, 17783–17795.